ACS APPLIED MATERIALS & INTERFACES

www.acsami.org

Research Article

Bi and Sb Codoped $Cs_2Ag_{0.1}Na_{0.9}InCl_6$ Double Perovskite with Excitation-Wavelength-Dependent Dual-Emission for Anti-Counterfeiting Application

Xiang Li, Shuhong Xu, Fan Liu, Junfeng Qu, Haibao Shao, Zhuyuan Wang, Yiping Cui, Dayan Ban, and Chunlei Wang*

Cite This: *ACS Appl. Mater. Interfaces* 2021, 13, 31031−31037

Read Online

ACCESS | Metrics & More | Article Recommendations | Supporting Information

ABSTRACT: The growing demands for optical anti-counterfeiting technology require the development of new environmentally friendly materials with single component, multimodal fluorescence and high stability. Herein, the Bi/Sb codoped $Cs_2Ag_{0.1}Na_{0.9}InCl_6$ lead-free double perovskite material is reported as an efficient multimodal luminescence material with excitation-wavelength-dependent emission. When excited by 360 nm UV light, dual-emission is observed at 455 and 560 nm, which comes from the $^3P_1-{}^1S_0$ transition of Sb^{3+} ions and self-trapped excitons (STEs), respectively. Under the 320 nm UV lamp, the microcrystals show only a blue emission centered at 455 nm. Therefore, the Bi/Sb codoped $Cs_2Ag_{0.1}Na_{0.9}InCl_6$ double perovskite emits blue and yellow lights under the 320 and 360 nm UV lamp, respectively. Moreover, the obtained double perovskite shows a high PLQY up to 41% and excellent stability against both air and high temperature, which make it a promising anti-counterfeiting material.

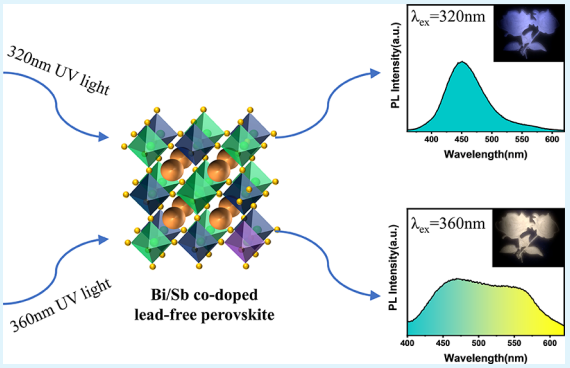

KEYWORDS: *double perovskite, lead-free, $Cs_2NaInCl_6$, excitation-wavelength-dependent emission, anti-counterfeiting*

INTRODUCTION

Fluorescence anti-counterfeiting materials, due to their high photoluminescence (PL) intensity/efficiency and tunable excitation/emission wavelength, are widely used in the fields of banknotes, artworks, documents, and even personal information security.[1−5] The traditional fluorescent anti-counterfeiting technology generally uses a single color fluorescent phosphor to print patterns,[6] which is far from meeting the requirements of practical applications. To further enhance the security of anti-counterfeiting technology, it is essential to develop more complex multicolor fluorescent anti-counterfeiting technologies. The currently common multicolor fluorescent anti-counterfeiting technology is to mix several organic materials with different excitation wavelengths and fluorescent colors.[7] When the excitation wavelength changes, different kinds of organic materials in the mixture are excited, thus showing excitation-wavelength-dependent fluorescent colors. The problem for the organic materials is the poor long-term stability, which limits the development of fluorescence anti-counterfeiting in practical application. Besides, the different relative temporal stability and undesirable changes of the chromaticity coordinates of mixture materials are always serious problems for the multiple components of anti-counterfeiting phosphor. One alternative and attractive approach to solve the above problems is to develop single-component phosphor materials with excitation-dependent multicolor emissions.

Because of its excellent optical properties, lead halide perovskite is expected as the newcomer material for anti-counterfeiting.[8−13] In recent years, researchers have made a variety of attempts to achieve dual-emission fluorescence of lead halide perovskites, such as metal ion doping[14−17] and bonding with metal−organic frameworks (MOFs).[18] However, these lead halide perovskite materials contain toxic lead ions with poor stability against high temperature, humidity, and oxygen.[19−22] These shortcomings not only limit their durable and large-scale applications but also bring potential pollution sources to the environment.[23−25] To solve this problem, various lead-free perovskite materials have been developed one after another. Among all lead-free perovskite materials, double perovskite is regarded as a promising alternative due to its good photoelectric properties and high stability.[26−28] The molecular formula of double perovskite can be written as

Received: April 29, 2021
Accepted: June 16, 2021
Published: June 23, 2021

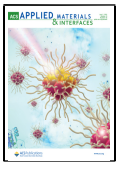

https://doi.org/10.1021/acsami.1c07809
ACS Appl. Mater. Interfaces 2021, 13, 31031−31037

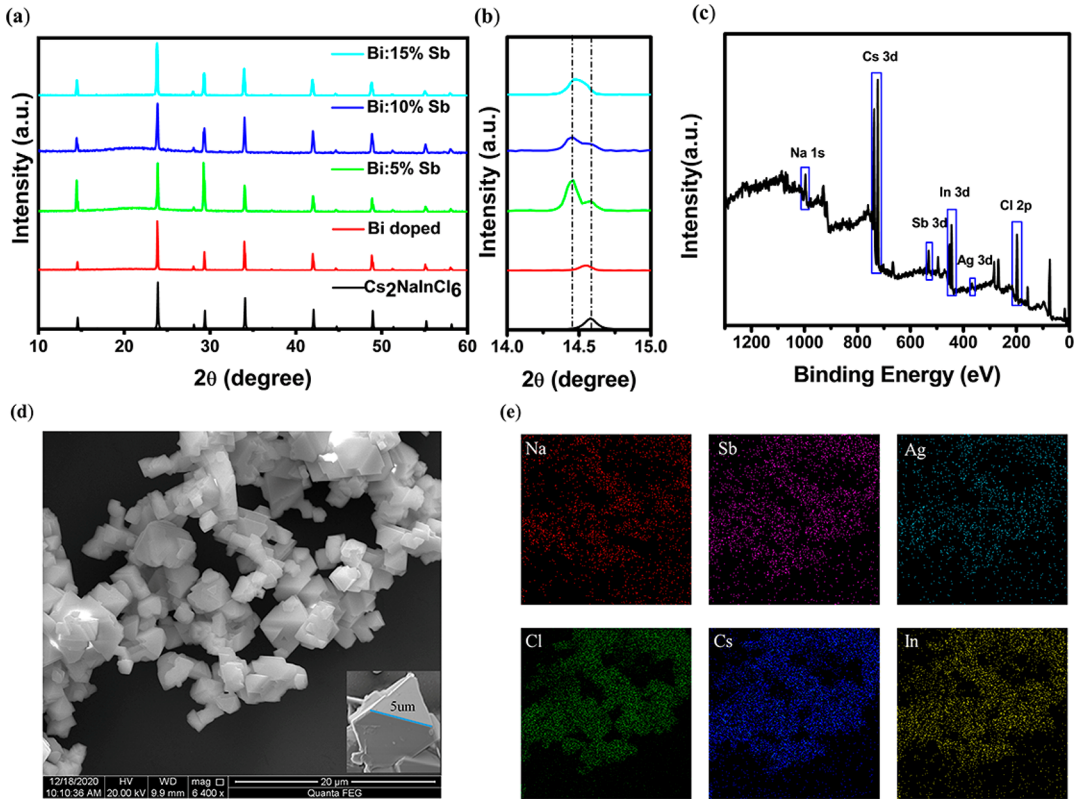

Figure 1. (a) XRD patterns and (b) magnified XRD patterns in the region of 14−15° $Cs_2Ag_{0.1}Na_{0.9}InCl_6$:(1% Bi, *x*% Sb) and $Cs_2NaInCl_6$; (c) XPS results, (d) SEM image, and (e) EDS mapping of $Cs_2Ag_{0.1}Na_{0.9}InCl_6$:(1% Bi, 10% Sb). The XRD pattern of $Cs_2NaInCl_6$ is the standard XRD spectrum from the Cambridge Crystallographic Data Centre (CCDC no. 1986198).

$A_2B^IB^{III}X_6$, which is characterized by a three-dimensional network of alternating corner-sharing $[B^IX_6]$ and $[B^{III}X_6]$ octahedra. To prepare polychromatic double perovskite, impurity ions such as Mn^{2+} are doped into double perovskite to achieve dual-emission fluorescence.[29−31] However, their polychromatic fluorescence is not excitation-wavelength-dependent, which is not up to the advanced anti-counterfeiting requirements. To prepare multimodal luminescence material, Du et al. reported $Yb^{3+}/Er^{3+}/Bi^{3+}$ codoped $Cs_2Ag_{0.6}Na_{0.4}InCl_6$, which produces yellow light of double perovskite matrix under ultraviolet light as well as up-conversion luminescence by absorbing near-infrared energy in $^4I_{13/2}$, $^4I_{11/2}$, $^4F_{9/2}$, and $^4F_{7/2}$ levels of sensitizer ion Yb^{3+}.[32] However, the high price and rare earth presence are not conducive to the application of rare-earth-based phosphors in anti-counterfeiting. Moreover, the quantum efficiency of up-conversion fluorescence is low, which has difficulty exceeding 5%.[33] Therefore, it is still urgent to find a more suitable ion doping method to obtain polychromatic double perovskite material with excitation-wavelength-dependent fluorescence for anti-counterfeiting, which is nontoxic, stable, and of high efficiency and low cost.

Herein, a Bi/Sb codoped $Cs_2Ag_{0.1}Na_{0.9}InCl_6$ lead-free double perovskite with excellent multimodal and polychromatic luminescence properties is reported. Through the introduction of Sb^{3+} ions, the fluorescence of $Cs_2Ag_{0.1}Na_{0.9}InCl_6$:Bi changes from one-peak emission to tunable dual-peak emission controlled by Sb^{3+} doping concentration. Most importantly, the excitation mode of Sb impurity fluorescence is completely independent, which leads to excitation-dependent fluorescence of Bi^{3+}/Sb^{3+} codoped $Cs_2Ag_{0.1}Na_{0.9}InCl_6$. When the excitation wavelength changes from 320 to 360 nm, the luminescence color changes from blue to light yellow. In addition, the highest fluorescence quantum yield reaches 41%, which is several times higher than the up-conversion efficiency of rare earth doped phosphor. Further experimental results also confirm the high stability of this material against air and high temperature. On the basis of its unique luminescent properties, $Cs_2Ag_{0.1}Na_{0.9}InCl_6$:(1% Bi, *x* % Sb) may be a promising anti-counterfeiting material.

RESULTS AND DISCUSSION

Morphology and Structure. The results of the XRD, XPS, SEM, and EDS measurements of the as-prepared phosphors are shown in Figure 1. As shown in Figure 1a, XRD measurement of $Cs_2Ag_{0.1}Na_{0.9}InCl_6$:(1% Bi, 0−15% Sb) samples can well correspond to the $Cs_2NaInCl_6$ phase. The XRD patterns of the phosphors with different Sb contents remain almost unchanged, and it means that the Sb doping does not seriously change the host crystal structure. The representative XRD peak of the codoped sample exhibits a slight shift as compared to that of the sample without Sb doping (see Figure 1b), indicating that Sb is successfully incorporated into the host material. According to the literature, Sb^{3+} has larger size in crystal lattice than In^{3+} due to the bond instability effect of the ns^2 lone pair.[34,35] As a result, the diffraction peak shifts to a low angle with the increasing content of Sb.

To further confirm the presence of dopants, the $Cs_2Ag_{0.1}Na_{0.9}InCl_6$:(1% Bi, 10% Sb) sample was measured by XPS. The survey XPS spectrum (Figure 1c) shows characteristic peaks of Cs, Na, Ag, In, Cl, and Sb. As shown in Figure S1, 367.62 and 373.96 eV peaks corresponding to the 3d energy

https://doi.org/10.1021/acsami.1c07809
ACS Appl. Mater. Interfaces 2021, 13, 31031−31037

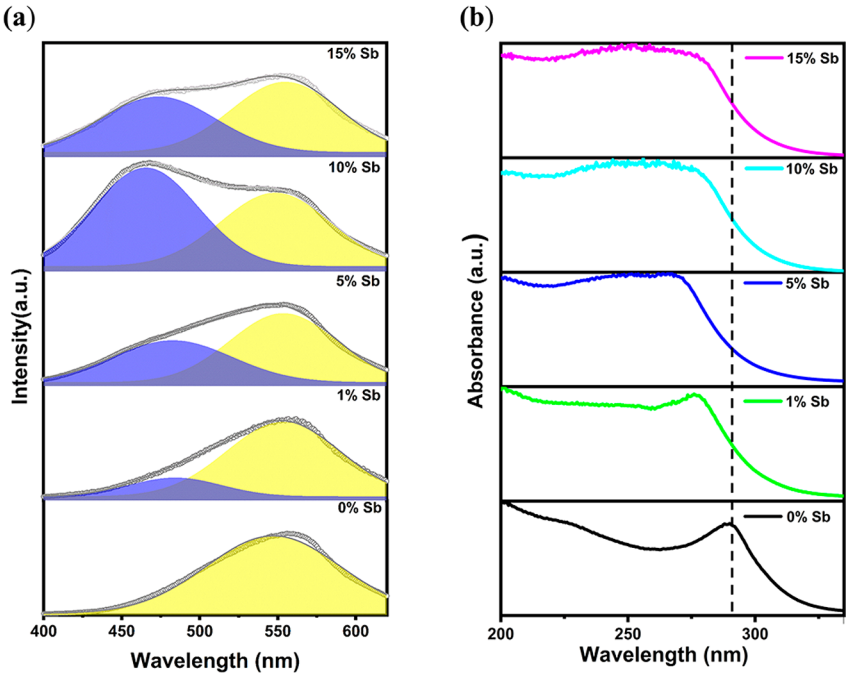

Figure 2. (a) PL spectra (excited by 350 nm UV-light) and (b) UV−vis absorption spectra of $Cs_2Ag_{0.1}Na_{0.9}InCl_6$:1% Bi powder with different Sb content.

level of Ag^+ were detected in the sample. The peaks at 198.1 and 199.9 eV correspond to the Cl $2p_{3/2}$ and Cl $2p_{1/2}$ levels.[36] The peaks at 724.05 and 738.05 eV correspond to the 3d doublet of Cs^+. The peak at 1071.38 eV corresponds to the 1s level of Na^+. The peaks at 445.49 and 453.05 eV correspond to the 3d doublet of In^{3+}. The peaks at 532.9 and 540.0 eV correspond to the $3d_{5/2}$ and $3d_{3/2}$ levels of Sb^{3+}, respectively. There are additional peaks at 531.7 and 535 eV, which can be attributed to the oxygen species on the crystal surface due to the surface.[37−40] We speculate that Sb^{3+} has been incorporated into the $Cs_2Ag_{0.1}Na_{0.9}InCl_6$:Bi matrix successfully. To confirm the presence of Bi, an inductively coupled plasma optical emission spectrometer (ICP-OES) was applied. The results confirm the presence of Bi in the final production in Table S1.

The SEM image (Figure 1d) shows that the obtained phosphor contained octahedral particles 2−5 μm in size. The well faceted shapes additionally verify the high crystallinity of the synthesized sample. Next, the EDS mapping was performed to verify the composition of the $Cs_2Ag_{0.1}Na_{0.9}InCl_6$:(1% Bi, 10% Sb) sample by collecting Cs, Ag, In, Cl, Na, Bi, and Sb signatures. As shown in Figure 1e, these six elements are evenly distributed over grains and perfectly covered each other, demonstrating the uniform composition of the microcrystals. Meanwhile, the Bi element was not detected in the sample because of the very small real doping amount.[41]

Effects of Sb and Bi Dopants. To study the influence of impurities, the optical properties of microcrystals with different doping levels were compared. In Figure 2a, it can be seen from the fluorescence spectrum recorded under the 350 nm excitation that $Cs_2Ag_{0.1}Na_{0.9}InCl_6$:1% Bi exhibits a very wide emission band [full-width at half-maxima (fwhm) = 100 nm)] with the center at 560 nm, which is caused by self-trapped excitons. By introducing Sb^{3+}, an additional emission peak appears at about 455 nm, which is attributed to the $^3P_1-{}^1S_0$ transition of Sb^{3+} ions (Figure S2). The fitting results of PL lifetime monitored at 455 nm show that τ_1 = 52.2 ns and τ_2 = 740.6 ns (Table S2 and Figure S3), close to the reported values of the $Cs_2NaInCl_6$:Sb^{3+} system, with τ_1 = 90 ns and τ_2 = 1016 ns, which further show that the additional emission comes from Sb. It can be seen that the doping concentration of Sb^{3+} does not change the emission peak position, but changes the relative intensity of the two emission peaks. The results show that, when the Sb/(Sb + In + Bi) ratio is 0.1:1, the relative intensity of Sb fluorescence reaches the maximum. As shown in Figure 2b, $Cs_2Ag_{0.1}Na_{0.9}InCl_6$:1% Bi without Sb doping has an absorption peak at 290 nm. When the doping amount of Sb increases, the absorption peak shows a blue shift, and the intensity of absorption in the wavelength range of 230−270 nm is significantly enhanced, which is attributed to the band absorption of Sb^{3+}.

The optical properties of materials doped with different amounts of Bi and Ag are discussed. First, the fluorescence spectra of $Cs_2Ag_{0.1}Na_{0.9}InCl_6$:10% Sb with different Bi content were measured (Figures S4 and S5). It can be seen that the STEs emission of double perovskite almost disappears without Bi doping. This indicates that the effect of Bi is to enhance the STEs emission of perovskite, which is similar to that reported earlier. On the other hand, the fluorescence spectra of microcrystals with different Ag/(Ag+Na) feed ratios are presented in Figures S6 and S7. In these samples, the total amount of Ag+Na was fixed. From Figure S6, without doping Bi, simply changing the proportion of silver cannot form double peaks in the PL spectrum. Moreover, with increasing proportion of Ag, the blue luminescence intensity decreases. From Figure S7, with 1% Bi doping, the fluorescence spectrum of samples without silver impurity shows only the emission of Sb centered at 455 nm, meaning that double peaks appear only in the presence of both Bi and Ag. When the Ag/(Ag+Na) feed ratio increases to 0.2, the fluorescence is caused mainly by STEs emission of the host double perovskite. The dual-emission can be observed for the samples with an Ag/(Ag+Na)

https://doi.org/10.1021/acsami.1c07809
ACS Appl. Mater. Interfaces 2021, 13, 31031−31037

feed ratio of about 0.1. Therefore, the feeding amount of Ag has a significant effect on the intensity ratio of dual-emissions.

Excitation-Wavelength-Dependent Emission. As is shown in Figure 3a and b, the Sb doped microcrystals are characterized by excitation-wavelength-dependent emission. The samples without Sb doping have the same fluorescence centered at 560 nm under excitation from 320 to 360 nm. The fluorescence spectra of samples doped with 10% Sb show a dual-peak emission with the components at 455 and 560 nm, when the excitation wavelength ranges from 320 to 360 nm. As shown in Figure 3b, the intensity ratio of the peaks at 455 and 560 nm changes with the excitation wavelength. Also, the corresponding CIE coordinates (Figure S8) change from (0.16, 0.12) to (0.24, 0.34).

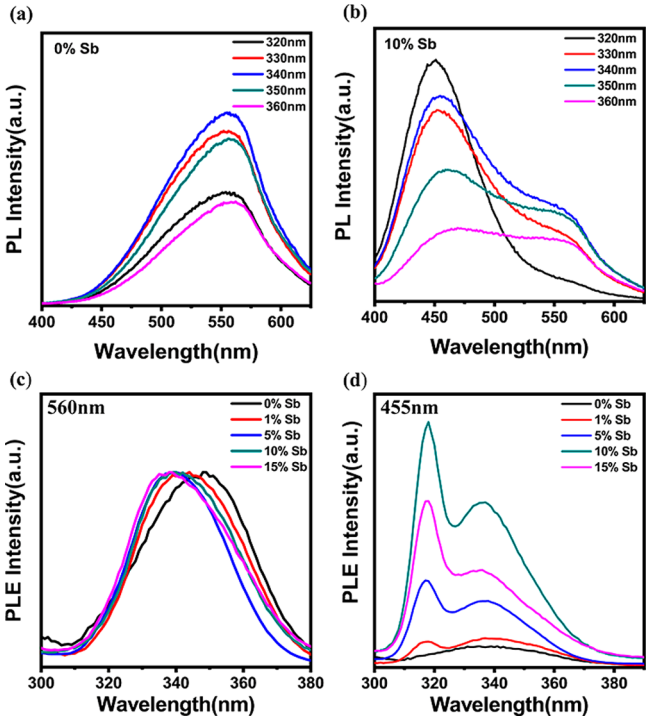

Figure 3. PL spectra (excitation wavelength ranges from 320 to 360 nm) of (a) $Cs_2Ag_{0.1}Na_{0.9}InCl_6$:1% Bi and (b) $Cs_2Ag_{0.1}Na_{0.9}InCl_6$:(1% Bi,10% Sb). (c) PLE (monitored the PL peak at 560 nm) and (d) PLE (monitored the PL peak at 455 nm) of $Cs_2Ag_{0.1}Na_{0.9}InCl_6$:1% Bi powder with different Sb content.

To further evaluate the cause of excitation-wavelength-dependent fluorescence, the excitation spectrum of $Cs_2Ag_{0.1}Na_{0.9}InCl_6$:(1% Bi, *x*% Sb) monitored at 455 and 560 nm was measured. For the excitation spectrum of STEs emission monitored at 560 nm (Figure 3c), the excitation spectrum of samples without Sb doping ranges from 310 to 380 nm, which comes from the absorption by the perovskite bandgap transitions, and the energy reaches the STE level through energy transfer. With the increase of Sb doping content, the range of excitation spectrum remains at 310−380 nm, indicating that Sb doping does not change the excitation approach of STEs emission. Meanwhile, a blue shift of excitation peak with the increase of Sb doping can be found, which is consistent with the blue shift of the absorption peak in the absorption spectrum (Figure 3a), indicating that Sb doping can slightly increase the bandgap width of perovskite.

For the excitation spectrum monitored at 455 nm (Figure 3d), the excitation spectrum continues to be over 310−380 nm, which is the same as that of the excitation spectrum monitored at 560 nm, indicating that the energy transfer from the perovskite conduction band to the Sb impurity level is one of the reasons for the Sb emission. Different from the excitation spectrum monitored at 560 nm, there are two maxima (at 317 and 337 nm) in the excitation spectrum monitored at 455 nm of the Sb doped samples,which is attributed to the Jahn teller splitting $5s^2 \rightarrow 5s^1p^1$ transition of the $[SbCl_6]^{3-}$ octahedron. This is consistent with the new absorption band induced by Sb doping in the above absorption spectra. Also, when the doping concentration of Sb is 10%, there will be optimal PLE intensity. The slight decrease in PLE

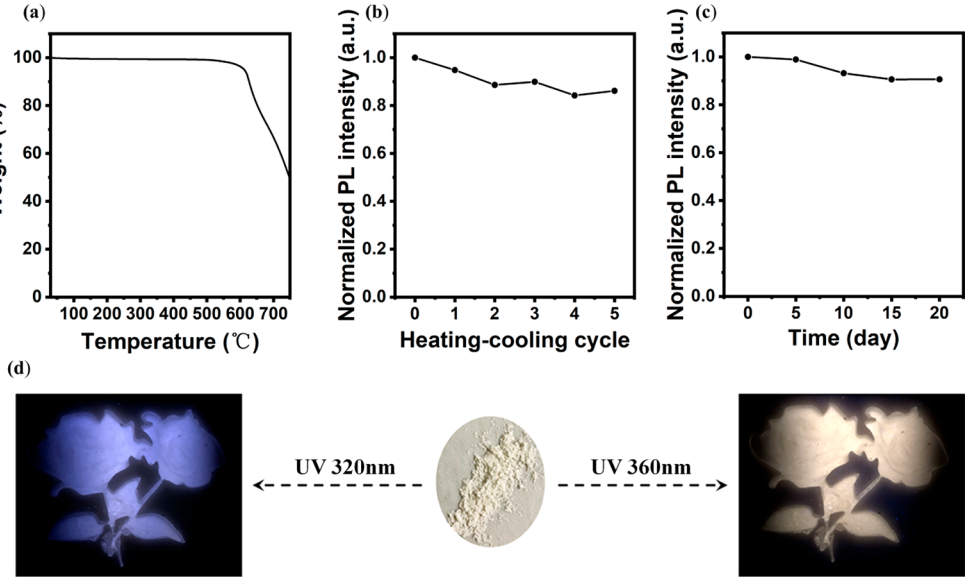

Figure 4. (a) Thermogravimetric analysis graphs. (b) Heating/cooling PL tests (the powder was heated on a hot plate at 598 K for 15 min, and then removed from the hot plate and used for measurement after cooling to 298 K). (c) PL stability measured in air without any encapsulation. (d) Photographs of $Cs_2Ag_{0.1}Na_{0.9}InCl_6$:(1% Bi, 10% Sb) encapsulated in the PS/toluene film irradiated by a UV lamp at 320 and 360 nm, respectively.

https://doi.org/10.1021/acsami.1c07809
ACS Appl. Mater. Interfaces 2021, 13, 31031−31037

intensity (monitored the PL peak at 455 nm) can be observed when the concentration continues to increase, suggesting concentration quenching begins to play a role for the higher Sb^{3+} content.[42,43] There are two excitation approaches for Sb emission, which can explain the excitation-wavelength-dependent emission (Figure S9). When excited by the 320 nm UV light, the emission of the STE state is weak due to the low excitation efficiency, while Sb related emission is strong due to the existence of two excitation approaches, leading to the fluorescence dominated by Sb related emission. When the excitation wavelength is 360 nm, there is only one excitation approach for Sb and STEs emission, leading to dual-emission broadband yellow fluorescence.

Stability and Anti-Counterfeiting Application. The thermal stability of $Cs_2Ag_{0.1}Na_{0.9}InCl_6$:(1% Bi, 10% Sb) was characterized by thermogravimetric (TG) analysis (Figure 4a). The TG curve shows that the sample is stable up to 500 °C, and there is no observable weight loss. When the temperature rises from 520 to 700 °C, the evaporation of the salts ($InCl_3$ and $BiCl_3$) characterized by low boiling points results in about 33% weight loss of the sample. As the temperature continues to rise, further weightlessness comes from the azeotropy of the residual molten salts. The thermal cycling test (298−598−298 K) in ambient air then was performed, and the integrated PL intensities were traced at 298 K. As shown in Figure 4b, after five cycles of continuous testing, the PL intensity exhibits ∼14% decay altogether, showing that these samples have excellent thermal stability to extend their application durability in a much harsher environment. The stability test of powder under UV lamp was complemented in Figure S10. As can be seen, after a continuous irradiation of 24 h, the PL intensity remained 80% as compared to the initial PL intensity. It is much superior to the conventional lead halide perovskites. To verify the stability of $Cs_2Ag_{0.1}Na_{0.9}InCl_6$:(1% Bi, *x*% Sb) against air, the phosphor with 10% Sb doping was exposed to the air and tested every 4 days, and the results are displayed in Figure 4c. After exposure to the air for 20 days, the fluorescence intensity of the perovskite can still reach 90.6%. Its remarkable stability indicates the reliability of $Cs_2Ag_{0.1}Na_{0.9}InCl_6$:(1% Bi, *x*% Sb) as commercial anti-counterfeiting fluorescent materials.

The PS/toluene solution is used to make the perovskite material into a flexible film to further present the versatility and applications of $Cs_2Ag_{0.1}Na_{0.9}InCl_6$:(1% Bi, *x*% Sb) material. The fluorescent anti-counterfeiting pictures are shown in Figure 4d. The flexible film shows blue and bright yellow patterns when irradiated by 320 and 360 nm UV light, respectively, and the luminous color in the pattern is evidently different. It is believed that this perovskite material is not easy to replicate because of its unique properties and can be used as an advanced anti-counterfeiting material in fluorescent anti-counterfeiting.

CONCLUSIONS

In this work, the Bi/Sb codoped $Cs_2Ag_{0.1}Na_{0.9}InCl_6$ lead-free double perovskite was successfully synthesized and displayed a dual-color luminescence from STEs and Sb-dopant emission. The relative emission intensity of the two peaks can be tuned by the doping concentration of Sb^{3+}. In addition, the bright blue and yellow fluorescent emissions can be clearly observed in the codoped sample excited by 320 and 360 nm UV irradiation. Its obvious excitation-wavelength-dependent fluorescence provides a significant feature for anti-counterfeiting recognition. Finally, Bi/Sb codoped $Cs_2Ag_{0.1}Na_{0.9}InCl_6$ lead-free double perovskite with high PLQY, low cost, and remarkable stability has been applied in fluorescent anti-counterfeiting. This toxic-element-free material provides a new directional solution for the development of environmentally friendly materials with excitation-wavelength-dependent fluorescence for high-level anti-counterfeiting technology.

EXPERIMENTAL SECTION

Materials. Cesium chloride (CsCl, Aladdin, 99.99%), silver chloride (AgCl, Macklin, 99.5%), sodium chloride (NaCl, Macklin, 99.5%), anhydrous bismuth chloride ($BiCl_3$, Macklin, 99.99%), indium acetate ($InAC_3$, Aladdin, 99.99%), and antimony acetate ($SbAC_3$, Aladdin, 97%) were used. Hydrochloric acid and ethanol were purchased from Sinopharm Chemical Reagent Co. All materials were used without further purification.

Synthesis of $Cs_2Ag_{0.1}Na_{0.9}InCl_6$:(1% Bi, *x*% Sb) Powder. For the synthesis of $Cs_2Ag_{0.1}Na_{0.9}InCl_6$:(1% Bi, *x*% Sb), starting materials containing 0.1 mmol of AgCl, 0.9 mmol of NaCl, (1−0.75) mmol of $InAc_3$, 0.01 mmol of $BiCl_3$, and varying amounts (0−0.15 mmol) of $SbAc_3$ were dissolved in 10 mL of HCl (12 mol/L) in a three-neck flask and continuously stirred in an oil bath at 80 °C for 30 min to form a clear solution. The total amount of In, Bi, and Sb should be 1 mmol, and the molar ratios of the Sb and Bi impurities are relative to this amount. One neck of the double flask was connected to the condenser tube to prevent the evaporation of HCl. After the starting materials were completely dissolved, 2 mmol of CsCl powder was added into the transparent solution under stirring to form a light white precipitate immediately. The mixture was stirred continuously for 2 h to ensure complete recrystallization. The precipitate was then filtered and washed with ethanol. After centrifugation, the precipitate was dried in a 100 °C vacuum oven for 12 h. The dried samples were used for further characterization.

Fabrication of $Cs_2Ag_{0.1}Na_{0.9}InCl_6$:(1% Bi, *x*% Sb) PS/Toluene Film. Transparent polystyrene (PS)/toluene solution was obtained by mixing PS (2.0 g) and toluene (5 mL) and dissolving them completely. A certain amount of previously prepared double perovskite microcrystalline powder was redispersed in 1 mL of toluene, injected into PS/toluene solution, and stirred for 10 min. The solution was then added to the template, dried in air at room temperature for 2 h, and then heated to 50 °C in an oven for 30 min to remove any residual solvent, resulting in a patterned film.

Characterization. The PLQY and luminescence decay curves of phosphors were measured with the use of an Edinburgh FLS1000. Photoluminescence (PL) and photoluminescence excitation spectra (PLE) measurements were performed with a Shimadzu RF-5301 PC spectrofluorimeter. The excitation wavelength ranged from 320 to 360 nm. For the PLE measurement, emission peak wavelengths of 455 and 560 nm were selected. The ICP-OES analyses were performed with a SPECTROBLUE ICP-OES. Thermogravimetric (TG) analyses were carried out in the "Mettler TGA/SDTA 851e" thermal analyzer at a heating rate of 10 °C/min. The UV−vis absorption spectra and transmittance were recorded with a Shimadzu 3600 UV−vis near-infrared spectrophotometer. X-ray photoelectron spectroscopy (XPS) and X-ray powder diffraction (XRD) were carried out using a Thermos Scientific ESCAlab 250xi spectrometer with monochromatized Al Kα as the X-ray source. Scanning electron microscope (SEM) and energy dispersive spectrometer (EDS) images were collected with a Quanta 200 from FEI.

ASSOCIATED CONTENT

Supporting Information

The Supporting Information is available free of charge at https://pubs.acs.org/doi/10.1021/acsami.1c07809.

High-resolution XPS spectra, time-resolved PL curves and PL stability under the UV lamp of $Cs_2Ag_{0.1}Na_{0.9}InCl_6$:(1% Bi,10% Sb), ICP-OES results

https://doi.org/10.1021/acsami.1c07809
ACS Appl. Mater. Interfaces 2021, 13, 31031−31037

of $Cs_2Ag_{0.1}Na_{0.9}InCl_6$:(4% Bi,10% Sb), and PL analysis of samples with different Bi and Ag content (PDF)

AUTHOR INFORMATION

Corresponding Author

Chunlei Wang − *Advanced Photonics Center, School of Electronic Science and Engineering, Southeast University, Nanjing 210096, People's Republic of China;* orcid.org/0000-0002-7675-8921; Email: wangchl@seu.edu.cn

Authors

Xiang Li − *Advanced Photonics Center, School of Electronic Science and Engineering, Southeast University, Nanjing 210096, People's Republic of China*

Shuhong Xu − *Advanced Photonics Center, School of Electronic Science and Engineering, Southeast University, Nanjing 210096, People's Republic of China*

Fan Liu − *Advanced Photonics Center, School of Electronic Science and Engineering, Southeast University, Nanjing 210096, People's Republic of China*

Junfeng Qu − *Advanced Photonics Center, School of Electronic Science and Engineering, Southeast University, Nanjing 210096, People's Republic of China*

Haibao Shao − *School of Electronics & Information, Nantong University, Nantong 226019, People's Republic of China*

Zhuyuan Wang − *Advanced Photonics Center, School of Electronic Science and Engineering, Southeast University, Nanjing 210096, People's Republic of China;* orcid.org/0000-0003-1262-5342

Yiping Cui − *Advanced Photonics Center, School of Electronic Science and Engineering, Southeast University, Nanjing 210096, People's Republic of China;* orcid.org/0000-0002-4648-2506

Dayan Ban − *Waterloo Institute for Nanotechnology and Department of Electrical and Computer Engineering, University of Waterloo, Waterloo, Ontario N2L 3G1, Canada*

Complete contact information is available at: https://pubs.acs.org/10.1021/acsami.1c07809

Notes

The authors declare no competing financial interest.

ACKNOWLEDGMENTS

We thank the SEU-FEI Nano-Pico Center for SEM characterization. This work is supported by the Natural Science Foundation of China (no. 61535003), the Natural Science Foundation of China (grant nos. 22075043, 21875034, and 61704093), and the Foundation of Jiangsu Province for Outstanding Young Teachers in University (grant no. BK20180064).

REFERENCES

(1) Yoon, B.; Lee, J.; Park, I. S.; Jeon, S.; Lee, J.; Kim, J.-M. Recent Functional Material Based Approaches to Prevent and Detect Counterfeiting. *J. Mater. Chem. C* **2013**, *1* (13), 2388−2403.

(2) Kumar, P.; Singh, S.; Gupta, B. K. Future Prospects of Luminescent Nanomaterial Based Security Inks: From Synthesis to Anti-Counterfeiting Applications. *Nanoscale* **2016**, *8* (30), 14297−14340.

(3) Zhao, Y.; Shi, C.; Yang, X.; Shen, B.; Sun, Y.; Chen, Y.; Xu, X.; Sun, H.; Yu, K.; Yang, B.; Lin, Q. pH- and Temperature-Sensitive Hydrogel Nanoparticles with Dual Photoluminescence for Bioprobes. *ACS Nano* **2016**, *10* (6), 5856−5863.

(4) Andres, J.; Hersch, R. D.; Moser, J. E.; Chauvin, A. S. A New Anti-Counterfeiting Feature Relying on Invisible Luminescent Full Color Images Printed with Lanthanide-Based Inks. *Adv. Funct. Mater.* **2014**, *24* (32), 5029−5036.

(5) Li, X.; Xie, Y.; Song, B.; Zhang, H. L.; Chen, H.; Cai, H.; Liu, W.; Tang, Y. A Stimuli-Responsive Smart Lanthanide Nanocomposite for Multidimensional Optical Recording and Encryption. *Angew. Chem., Int. Ed.* **2017**, *56* (10), 2689−2693.

(6) Han, S.; Bae, H. J.; Kim, J.; Shin, S.; Choi, S. E.; Lee, S. H.; Kwon, S.; Park, W. Lithographically Encoded Polymer Microtaggant Using High-Capacity and Error-Correctable QR Code for Anti-Counterfeiting of Drugs. *Adv. Mater.* **2012**, *24* (44), 5924−5929.

(7) Ataeefard, M.; Nourmohammadian, F. Producing Fluorescent Digital Printing Ink: Investigating the Effect of Type and Amount of Coumarin Derivative Dyes on the Quality of Ink. *J. Lumin.* **2015**, *167*, 254−260.

(8) Dirin, D. N.; Benin, B. M.; Yakunin, S.; Krumeich, F.; Raino, G.; Frison, R.; Kovalenko, M. V. Microcarrier-Assisted Inorganic Shelling of Lead Halide Perovskite Nanocrystals. *ACS Nano* **2019**, *13* (10), 11642−11652.

(9) Jiang, G.; Guhrenz, C.; Kirch, A.; Sonntag, L.; Bauer, C.; Fan, X.; Wang, J.; Reineke, S.; Gaponik, N.; Eychmuller, A. Highly Luminescent and Water-Resistant $CsPbBr_3$-$CsPb_2Br_5$ Perovskite Nanocrystals Coordinated with Partially Hydrolyzed Poly (Methyl Methacrylate) and Polyethylenimine. *ACS Nano* **2019**, *13* (9), 10386−10396.

(10) Zhang, F.; Shi, Z.; Li, S.; Ma, Z.; Li, Y.; Wang, L.; Wu, D.; Tian, Y.; Du, G.; Li, X.; Shan, C. Synergetic Effect of the Surfactant and Silica Coating on the Enhanced Emission and Stability of Perovskite Quantum Dots for Anticounterfeiting. *ACS Appl. Mater. Interfaces* **2019**, *11* (31), 28013−28022.

(11) Gao, A.; Yan, J.; Wang, Z.; Liu, P.; Wu, D.; Tang, X.; Fang, F.; Ding, S.; Li, X.; Sun, J.; Cao, M.; Wang, L.; Li, L.; Wang, K.; Sun, X. W. Printable $CsPbBr_3$ Perovskite Quantum Dot Ink for Coffee Ring-Free Fluorescent Microarrays Using Inkjet Printing. *Nanoscale* **2020**, *12* (4), 2569−2577.

(12) Sun, C.; Su, S.; Gao, Z.; Liu, H.; Wu, H.; Shen, X.; Bi, W. Stimuli-Responsive Inks Based on Perovskite Quantum Dots for Advanced Full-Color Information Encryption and Decryption. *ACS Appl. Mater. Interfaces* **2019**, *11* (8), 8210−8216.

(13) Wang, H.; Yao, W.; Tian, Q.; Li, M.; Tian, B.; Liu, L.; Wu, Z.; Wu, W. Printable Monodisperse All-Inorganic Perovskite Quantum Dots: Synthesis and Banknotes Protection Applications. *Adv. Mater. Technol.* **2018**, *3* (11), 1800150.

(14) Huang, G.; Wang, C.; Xu, S.; Zong, S.; Lu, J.; Wang, Z.; Lu, C.; Cui, Y. Postsynthetic Doping of $MnCl_2$ Molecules into Preformed $CsPbBr_3$ Perovskite Nanocrystals via a Halide Exchange-Driven Cation Exchange. *Adv. Mater.* **2017**, *29* (29), 1700095.

(15) Wu, H.; Xu, S.; Shao, H.; Li, L.; Cui, Y.; Wang, C. Single Component Mn-Doped Perovskite-Related $CsPb_2Cl_xBr_{5-x}$ Nanoplatelets with a Record White Light Quantum Yield of 49%: A New Single Layer Color Conversion Material for Light-Emitting Diodes. *Nanoscale* **2017**, *9* (43), 16858−16863.

(16) Wei, Q.; Li, M.; Zhang, Z.; Guo, J.; Xing, G.; Sum, T. C.; Huang, W. Efficient Recycling of Trapped Energies for Dual-Emission in Mn-Doped Perovskite Nanocrystals. *Nano Energy* **2018**, *51*, 704−710.

(17) Cao, F.; Yu, D.; Xu, X.; Cai, B.; Gu, Y.; Dong, Y.; Shen, Y.; Zeng, H. Water-Assisted Synthesis of Blue Chip Excitable 2D Halide Perovskite with Green-Red Dual Emissions for White LEDs. *Small Methods* **2019**, *3* (11), 1900365.

(18) Zhang, D.; Zhou, W.; Liu, Q.; Xia, Z. $CH_3NH_3PbBr_3$ Perovskite Nanocrystals Encapsulated in Lanthanide Metal-Organic Frameworks as a Photoluminescence Converter for Anti-Counterfeiting. *ACS Appl. Mater. Interfaces* **2018**, *10* (33), 27875−27884.

(19) Huang, S.; Li, Z.; Kong, L.; Zhu, N.; Shan, A.; Li, L. Enhancing the Stability of $CH_3NH_3PbBr_3$ Quantum Dots by Embedding in Silica

Spheres Derived from Tetramethyl Orthosilicate in "Waterless" Toluene. *J. Am. Chem. Soc.* **2016**, *138* (18), 5749−5752.
(20) Bella, F.; Griffini, G.; Correa-Baena, J.-P.; Saracco, G.; Gratzel, M.; Hagfeldt, A.; Turri, S.; Gerbaldi, C. Improving Efficiency and Stability of Perovskite Solar Cells with Photocurable Fluoropolymers. *Science* **2016**, *354*, 203−206.
(21) Niu, G.; Guo, X.; Wang, L. Review of Recent Progress in Chemical Stability of Perovskite Solar Cells. *J. Mater. Chem. A* **2015**, *3* (17), 8970−8980.
(22) Leijtens, T.; Eperon, G. E.; Noel, N. K.; Habisreutinger, S. N.; Petrozza, A.; Snaith, H. J. Stability of Metal Halide Perovskite Solar Cells. *Adv. Energy. Mater.* **2015**, *5* (20), 1500963.
(23) Zhang, X.; Zhang, Y.; Zhang, X.; Yin, W.; Wang, Y.; Wang, H.; Lu, M.; Li, Z.; Gu, Z.; Yu, W. W. Yb^{3+} and Yb^{3+}/Er^{3+} Doping for Near-Infrared Emission and Improved Stability of $CsPbCl_3$ Nanocrystals. *J. Mater. Chem. C* **2018**, *6* (37), 10101−10105.
(24) Chen, Q.; Wu, J.; Ou, X.; Huang, B.; Almutlaq, J.; Zhumekenov, A. A.; Guan, X.; Han, S.; Liang, L.; Yi, Z.; Li, J.; Xie, X.; Wang, Y.; Li, Y.; Fan, D.; Teh, D. B. L.; All, A. H.; Mohammed, O. F.; Bakr, O. M.; Wu, T.; Bettinelli, M.; Yang, H.; Huang, W.; Liu, X. All-Inorganic Perovskite Nanocrystal Scintillators. *Nature* **2018**, *561* (7721), 88−93.
(25) Xiao, Z.; Song, Z.; Yan, Y. From Lead Halide Perovskites to Lead-Free Metal Halide Perovskites and Perovskite Derivatives. *Adv. Mater.* **2019**, *31* (47), 1803792.
(26) Luo, J.; Wang, X.; Li, S.; Liu, J.; Guo, Y.; Niu, G.; Yao, L.; Fu, Y.; Gao, L.; Dong, Q.; Zhao, C.; Leng, M.; Ma, F.; Liang, W.; Wang, L.; Jin, S.; Han, J.; Zhang, L.; Etheridge, J.; Wang, J.; Yan, Y.; Sargent, E. H.; Tang, J. Efficient and Stable Emission of Warm-White Light from Lead-Free Halide Double Perovskites. *Nature* **2018**, *563* (7732), 541−545.
(27) Tang, H.; Xu, Y.; Hu, X.; Hu, Q.; Chen, T.; Jiang, W.; Wang, L.; Jiang, W. Lead-Free Halide Double Perovskite Nanocrystals for Light-Emitting Applications: Strategies for Boosting Efficiency and Stability. *Adv. Sci.* **2021**, *8* (7), 2004118.
(28) Yang, B.; Hong, F.; Chen, J.; Tang, Y.; Yang, L.; Sang, Y.; Xia, X.; Guo, J.; He, H.; Yang, S.; Deng, W.; Han, K. Colloidal Synthesis and Charge-Carrier Dynamics of $Cs_2AgSb_{1-y}Bi_yX_6$ (X: Br, Cl; $0 \leq y \leq 1$) Double Perovskite Nanocrystals. *Angew. Chem., Int. Ed.* **2019**, *58* (8), 2278−2283.
(29) Chen, N.; Cai, T.; Li, W.; Hills-Kimball, K.; Yang, H.; Que, M.; Nagaoka, Y.; Liu, Z.; Yang, D.; Dong, A.; Xu, C. Y.; Zia, R.; Chen, O. Yb- and Mn-Doped Lead-Free Double Perovskite Cs_2AgBiX_6 ($X = Cl^-, Br^-$) Nanocrystals. *ACS Appl. Mater. Interfaces* **2019**, *11* (18), 16855−16863.
(30) Liu, X.; Xu, X.; Li, B.; Yang, L.; Li, Q.; Jiang, H.; Xu, D. Tunable Dual-Emission in Monodispersed Sb^{3+}/Mn^{2+} Codoped $Cs_2NaInCl_6$ Perovskite Nanocrystals through an Energy Transfer Process. *Small* **2020**, *16* (31), 2002547.
(31) Hu, M.; Luo, J.; Li, S.; Liu, J.; Li, J.; Tan, Z.; Niu, G.; Wang, Z.; Tang, J. Broadband Emission of Double Perovskite $Cs_2Na_{0.4}Ag_{0.6}In_{0.995}Bi_{0.005}Cl_6$: Mn^{2+} for Single-Phosphor White-Light-Emitting Diodes. *Opt. Lett.* **2019**, *44* (19), 4757−4760.
(32) Zeng, Z.; Huang, B.; Wang, X.; Lu, L.; Lu, Q.; Sun, M.; Wu, T.; Ma, T.; Xu, J.; Xu, Y.; Wang, S.; Du, Y.; Yan, C. H. Multimodal Luminescent $Yb^{3+}/Er^{3+}/Bi^{3+}$-Doped Perovskite Single Crystals for X-ray Detection and Anti-Counterfeiting. *Adv. Mater.* **2020**, *32* (43), 2004506.
(33) Sun, T.; Li, Y.; Ho, W. L.; Zhu, Q.; Chen, X.; Jin, L.; Zhu, H.; Huang, B.; Lin, J.; Little, B. E.; Chu, S. T.; Wang, F. Integrating Temporal and Spatial Control of Electronic Transitions for Bright Multiphoton Upconversion. *Nat. Commun.* **2019**, *10* (1), 1811.
(34) Gray, M. B.; Hariyani, S.; Strom, T. A.; Majher, J. D.; Brgoch, J.; Woodward, P. M. High-Efficiency Blue Photoluminescence in the $Cs_2NaInCl_6$:Sb^{3+} Double Perovskite Phosphor. *J. Mater. Chem. C* **2020**, *8* (20), 6797−6803.
(35) Jing, Y.; Liu, Y.; Jiang, X.; Molokeev, M. S.; Lin, Z.; Xia, Z. Sb^{3+} Dopant and Halogen Substitution Triggered Highly Efficient and Tunable Emission in Lead-Free Metal Halide Single Crystals. *Chem. Mater.* **2020**, *32* (12), 5327−5334.
(36) Bekenev, V. L.; Khyzhun, O. Y.; Sinelnichenko, A. K.; Atuchin, V. V.; Parasyuk, O. V.; Yurchenko, O. M.; Bezsmolnyy, Y.; Kityk, A. V.; Szkutnik, J.; CaŁus, S. Crystal growth and the electronic structure of Tl_3PbCl_5. *J. Phys. Chem. Solids* **2011**, *72* (6), 705−713.
(37) Li, J.; Tan, Z.; Hu, M.; Chen, C.; Luo, J.; Li, S.; Gao, L.; Xiao, Z.; Niu, G.; Tang, J. Antimony Doped Cs_2SnCl_6 with Bright and Stable Emission. *Front. Optoelectron.* **2019**, *12* (4), 352−364.
(38) Atuchin, V. V.; Isaenko, L. I.; Kesler, V. G.; Tarasova, A. Y. Single crystal growth and surface chemical stability of KPb2Br$_5$. *J. Cryst. Growth* **2011**, *318* (1), 1000−1004.
(39) Atuchin, V. V.; Isaenko, L. I.; Kesler, V. G.; Pokrovsky, L. D.; Tarasova, A. Y. Electronic parameters and top surface chemical stability of $RbPb_2Br_5$. *Mater. Chem. Phys.* **2012**, *132* (1), 82−86.
(40) Atuchin, V. V.; Goloshumova, A. A.; Isaenko, L. I.; Jiang, X.; Lobanov, S. I.; Zhang, Z.; Lin, Z. Crystal growth and electronic structure of low-temperature phase $SrMgF_4$. *J. Solid State Chem.* **2016**, *236*, 89−93.
(41) Li, S.; Shi, Z.; Zhang, F.; Wang, L.; Ma, Z.; Wu, D.; Yang, D.; Chen, X.; Tian, Y.; Zhang, Y.; Shan, C.; Li, X. Ultrastable Lead-Free Double Perovskite Warm-White Light-Emitting Devices with a Lifetime above 1000 h. *ACS Appl. Mater. Interfaces* **2020**, *12* (41), 46330−46339.
(42) Chen, B.; Wang, F. Combating Concentration Quenching in Upconversion Nanoparticles. *Acc. Chem. Res.* **2020**, *53* (2), 358−367.
(43) Nag, A.; Chakraborty, S.; Sarma, D. D. To Dope Mn^{2+} in a Semiconducting Nanocrystal. *J. Am. Chem. Soc.* **2008**, *130* (32), 10605−10611.

https://doi.org/10.1021/acsami.1c07809
ACS Appl. Mater. Interfaces 2021, 13, 31031−31037